# The $n$-th Power Fourier Spectrum Analysis for the Generalized Seismic Wavelets

Xuan Ke, Ying Shi, Xiaofei Fu, Liwei Song, Hongliang Jing, Jingbo Yang, and Zhen Zhang

***Abstract*—The generalized seismic wavelets (GSW) are defined by fractional derivatives of the Gaussian function, whose asymmetry allows them to represent seismic signals more accurately than the commonly used symmetrical Ricker wavelet. The latter is a particular case with a second derivative of the Gaussian function. To better obtain the GSW, which could be well-matched with seismic signals, this paper proposes the $n$-th power Fourier spectrum analysis method for GSW. Firstly, based on the $n$-th power Fourier spectrum of GSW, the proposed method builds the mathematical relationship between frequency characteristics (e.g., central frequency and bandwidth) and the statistical properties (e.g., mean frequency and deviation). Secondly, according to the $n$-th power Fourier spectrum, we propose a weighting calculation method for the derivative order $u$ of the Gaussian function. This method could be used for estimating GSW matched the seismic first arrival record, which is conducive to improving the accuracy of seismic imaging, inversion, and Q analysis. In theory, our proposed weighting method has better robustness and noise resistance than the traditional spectrum analysis method based on the power or amplitude spectrum. The experiment of synthetic noise-including first arrival record and vertical seismic profiling (VSP) field data, shows the effectiveness of the proposed approach.**

***Index Terms*—$n$-th power Fourier spectrum, generalized seismic wavelets, numerical solution.**

## I. Introduction

RICKER wavelet proposed by Ricker [1]–[3] has been widely used for seismic data processing. However, the symmetrical waveform of the Ricker wavelet is rare in nature. In addition, its definition and application of frequency parameters are still controversial [4]. In practice, wavelets that are well-matched to field signals often play essential roles in seismic data analysis, such as stable Q analysis [5], [6], seismic data modeling [7]–[9], reverse time migration [10]–[14], full-waveform inversion [15]–[17]. The simple symmetrical Ricker wavelet is unsuitable for these applications. So, more generalized wavelet should be adopted to achieve better results in seismic data processing.

Effective seismic wavelet estimation methods can help address the problems mentioned above. Generally, these methods can be divided into two main categories: deterministic and statistical. Deterministic methods need to combine with well data [18] and are typically solved using least-squares or spectral division methods [19], [20]. Statistical methods, on the other hand, estimate the seismic wavelet from the seismic data alone [21]. However, the earth's response can influence the statistical properties of the wavelet unpredictably. To address this issue, geophysicists have proposed several approaches to enhance the robustness of wavelet estimation methods [22]–[25].

Wang proposed a mathematical model for constructing seismic wavelets called GSW. They are defined by various derivatives of a Gaussian potential function and show various waveforms in the time domain, which are conducive to matching the seismic recording [26]. In the frequency domain, the different derivatives of the Gaussian function could be understood as the Gaussian spectrum multiplied by frequency-related factors $\omega^u$, where $\omega$ is the angular frequency and $u$ is the order of the derivative. This characteristic in the frequency domain can physically represent the frequency-dependent attenuation of the seismic wave when propagating through viscoelastic media. This demonstrates that the GSW are suitable for estimating the field wavelet signals both mathematically and physically. Furthermore, GSW have also been recently used for calculating the depth-domain seismic wavelet [25], detecting Karst voids based on dominant frequencies of seismic profiles [27], and Q-factor estimation [28]. Therefore, research on GSW extraction methods with more stability and noise resistance positively impacts seismic data processing.

Frequency analysis is a classical approach for estimating the best-matched wavelets with seismic recording and extracting the frequency parameters. In general, amplitude [29]–[31] and power spectra [32] are commonly used in frequency analysis, because they have clear physical meaning. Among them, with the help of the Lambert $W$ function [33], [34], the power spectrum analysis method of the GSW proposed by Wang [35] clearly illustrates the mathematical relationship between the frequency characteristics and statistical properties. However, this analysis method only focuses on the amplitude and power spectra, which are the first and quadratic power of the modulus

Xuan Ke, Ying Shi are with 1. School of Earth Science, Northeast Petroleum University, Daqing 163318, China (e-mail: kexuan@nepu.edu.cn; shiying@nepu.edu.cn); 2.Heilongjiang Provincial Key Laboratory of Oil and Gas Geophysical Exploration 3.National Engineering Research Center of Offshore Oil and Gas Exploration, Beijing 100027, China; 4.Key Laboratory of Oil and Gas Reservoir Formation Mechanism and Resource Evaluation, Northeast Petroleum University, Daqing 163318, China; 5.Key Laboratory of Continental Shale Hydrocarbon Accumulation and Efficient Development, Ministry of Education, Northeast Petroleum University, Daqing 163318, China.

Xiaofei Fu is with Institute of Unconventional Oil and Gas, Northeast Petroleum University, Daqing, 163318, China(e-mail: 760136897@qq.com)

Liwei Song is with School of Physics and Electronic Engineering, Northeast Petroleum University, Daqing 163318, China(e-mail: zhidao90@163.com)

Hongliang Jing is with Research and Development Center, BGP Inc., CNPC, Zhuozhou 072750,China(e-mail:jinghongliang@cnpc.com.cn)

Jingbo Yang is with Exploration Division, PetroChina Tarim Oilfield Company, Korla 841000, China(e-mail:yjingb-tlm@petrochina.com.cn)

Zhen Zhang is with Research Institute of Exploration and Development, PetroChina Tarim Oilfield Company, Korla 841000, China (e-mail:zzhen-tlm@petrochina.com.cn)

of Fourier spectra. It is not sufficiently generalized to consider other power numbers of the Fourier spectrum. Additionally, using a single power spectrum analysis method may introduce errors when the data contains noise. To address these issues, this paper extends the spectrum analysis method of the GSW [26] from the power spectrum analysis to the $n$-th power Fourier spectrum analysis. By introducing an arbitrary power number $n$ of the Fourier spectrum, this paper deduces the clear mathematical relationship between frequency characteristics and statistical properties, in which the latter depends on both the derivative order of the Gaussian function and the power number $n$ of the Fourier spectrum. This means that the arbitrary $n$-th power Fourier spectrum could be used for frequency analysis, estimating and matching the GSW with the seismic signals, not limited to using the amplitude or power spectrum. More importantly, according to the proposed weighting method, the potential error of using a single power spectrum analysis method can be avoided considering the spectrum analysis results of different power orders. Additionally, the proposed method allows for accurately determining the power number $n$ for the GSW, ensuring that the mean and central frequencies are almost equal. This is a theoretical extension of Wang's [26] viewpoint that the mean frequency obtained by the power spectrum is closer to the central frequency of the wavelet than the one received by the amplitude spectrum [36]. At last, the effectiveness of the proposed measure is finally verified through wavelet estimation for synthetic noise-including first arrival record and VSP field data

This article includes five sections in addition to the introduction:

(1) The first section mainly reviews the GSW and frequency characteristics which serve as the theoretical background of this paper.

(2) The second section introduces the theory of $n$-th power Fourier spectrum analysis for the GSW, which establishes the mathematical relationship between frequency characteristics and statistical properties of $n$-th power Fourier spectrum.

(3) The third section tells the weighting algorithm of $n$-th power Fourier spectrum, which provides the theoretical guidance for the practical application of this method.

(4) The fourth section includes synthetic and field examples to demonstrate the validity of our method.

(5) The fifth section offers conclusions and discussions about the proposed method.

## II. GSW and Frequency Characteristics

This section mainly reviews the GSW and the power spectrum analysis proposed by Wang [26]. Firstly, a potential function in negative Gaussian is introduced as follows:

$$g(\tau) = -\sqrt{\pi}\omega_0 exp\left[-\frac{\omega_0^2}{4}\left(\tau-\tau_0\right)^2\right], \tag{1}$$

where $\tau$ represents time in seconds, $\tau_0$ is the parameter to adjust the time position of the symmetrical axis and $\omega_0$ denotes the reference angular frequency, which is in radians per second.

The GSW could be expressed as the fractional derivatives of the negative Gaussian in the time domain [37]:

$$g^{(u)}(\tau) = \frac{1}{\Gamma(m-u)}\int_0^{\tau}(\tau-\xi)^{m-u-1}\, g^{(m)}(\xi)d\xi, \tag{2}$$

where $m$ is an integer, $g^{(m)}$ is the $m$-th order partial derivative of $g(\tau)$ with respect to $\tau$. The $u$ is a fraction between $[m-1, m)$ and $g^{(u)}(\tau)$ is the $u$-th fraction-order partial derivative of $g(\tau)$ with respect to $\tau$. The $\Gamma()$ represents the Gamma function. When the reference frequency $\omega_0$ and time position parameter $\tau_0$ are given, with the change of partial derivative order $u$, the GSW could be shown as the waveform with different phases, which can help the GSW match the seismic trace record in the time domain.

The normalized spectrum and amplitude spectrum of the GSW educed with the Fourier transform could be expressed as follows [26]:

$$\begin{aligned}\Phi^{(u)}(\omega) = (\frac{u}{2})^{-\frac{u}{2}}\frac{\omega^u}{\omega_0^u}exp\left(-\frac{\omega^2}{\omega_0^2}+\frac{u}{2}\right)\cdot \\ exp\left[-i\omega\tau_0 + i\pi\left(1+\frac{u}{2}\right)\right],\end{aligned} \tag{3}$$

$$\left|\Phi^{(u)}(\omega)\right| = \left(\frac{u}{2}\right)^{-\frac{u}{2}}\frac{\omega^u}{\omega_0^u}exp\left(-\frac{\omega^2}{\omega_0^2}+\frac{u}{2}\right). \tag{4}$$

If set the derivative of the amplitude spectrum $\left|\Phi^{(u)}(\omega)\right|$ with respect to the frequency $\omega$ to zero, after some derivations, the peak frequency could be expressed as follows:

$$\omega_p = \omega_0\sqrt{\frac{u}{2}}. \tag{5}$$

When the amplitude is set as 1/2, we substitute it into equation (4), we can obtain the following:

$$\left(\frac{2}{u}\right)^{\frac{u}{2}}\frac{\omega^u}{\omega_0^u}exp\left(-\frac{\omega^2}{\omega_0^2}+\frac{u}{2}\right) = \frac{1}{2}. \tag{6}$$

After some derivations, equation (6) could be rewritten as follows:

$$-\frac{2}{u}\frac{\omega^2}{\omega_0^2}exp\left(-\frac{2}{u}\frac{\omega^2}{\omega_0^2}\right) = -\frac{1}{2^{2/u}e}, \tag{7}$$

where $e$ is the Euler number and equation (7) could be seen as an inverse exponential equation form as follows:

$$zexp\left(z\right) = x. \tag{8}$$

The Lambert $W$ function could be introduced to solute equation (8) [26], [34], [35], [38]:

$$z = W\left(x\right). \tag{9}$$

Therefore, the solution of equation (7) is:

$$W\left(-\frac{1}{2^{2/u}e}\right) = -\frac{2}{u}\frac{\omega^2}{\omega_0^2}. \tag{10}$$

For $x = -\frac{1}{2^{2/u}e} < 0$, the Lambert $W$ function has two branches: $W_{-1}\left(x\right) \le -1$ and $W_0\left(x\right) \ge -1$. Therefore, we could obtain the analytic solution of equation (10) on each of the two Lambert $W$ function branches as follows:

$$\omega_{l1} = \omega_0\sqrt{-\frac{u}{2}W_0\left(-\frac{1}{2^{2/u}e}\right)}, \tag{11}$$

$$\omega_{l2} = \omega_0 \sqrt{-\frac{u}{2} W_{-1}\left(-\frac{1}{2^{2/u}e}\right)}, \tag{12}$$

from which, the half-bandwidth $\omega_b$ and the center of the frequency band $\omega_c$ could be determined as follows:

$$\omega_c = \frac{\omega_0}{2}\left[\sqrt{-\frac{u}{2} W_{-1}\left(-\frac{1}{2^{2/u}e}\right)} + \sqrt{-\frac{u}{2} W_{0}\left(-\frac{1}{2^{2/u}e}\right)}\right], \tag{13}$$

$$\omega_b = \frac{\omega_0}{2}\left[\sqrt{-\frac{u}{2} W_{-1}\left(-\frac{1}{2^{2/u}e}\right)} - \sqrt{-\frac{u}{2} W_{0}\left(-\frac{1}{2^{2/u}e}\right)}\right]. \tag{14}$$

In this section, we review the frequency characteristics of the GSW [26] and use them to derive an analytical expression for the GSW. In the following section, we propose an $n$-th Fourier spectrum analysis algorithm and build the mathematical relationship between the frequency characteristics and the statistical properties of GSW. The statistical properties of the field signal can be used as an initial frequency analysis parameter, and the derived mathematical relationship can help us derive the corresponding GSW expression.

## III. Statistical Properties of $n$-th Power Spectrum

Spectrum analysis of signals typically involves calculating the amplitude and power spectra, which are the first and second powers of the Fourier spectrum, respectively. If we extend this concept to the $n$-th power spectrum and apply it to the spectrum analysis of the GSW, we can obtain the $n$-th power Fourier spectra of the GSW as follows:

$$\begin{aligned} \left|\Phi^{(u)}(\omega)\right|^n &= \left(\frac{u}{2}\right)^{-\frac{nu}{2}} \frac{\omega^{nu}}{\omega_0^{nu}} exp\left(-\frac{n\omega^2}{\omega_0^2} + \frac{nu}{2}\right) \\ &= \left(\frac{2}{u}\right)^{\frac{nu}{2}} \frac{\omega^{nu}}{\omega_0^{nu}} exp\left(-\frac{n\omega^2}{\omega_0^2} + \frac{nu}{2}\right), \end{aligned} \tag{15}$$

where we only need to consider $\omega \geq 0$ and $u > 0$. If we set $n$ to 1, the expression in equation (15) reduces to the amplitude spectrum of the GSW, as expressed in equation (4). If we set $n$ to 2, the expression in equation (15) reduces to the power spectrum of the GSW.

Define the three definite integrals $D_I$, $D_{II}$ and $D_{III}$ as follows (they are derived in Appendix):

$$\begin{aligned} D_I &= \int_0^\infty \left|\Phi^{(u)}(\omega)\right|^n d\omega \\ &= \left(\frac{2}{nu}\right)^{\frac{nu}{2}} \frac{exp\left(\frac{nu}{2}\right)\omega_0}{2\sqrt{n}} \Gamma\left(\frac{nu}{2} + \frac{1}{2}\right), \end{aligned} \tag{16}$$

$$\begin{aligned} D_{II} &= \int_0^\infty \omega \left|\Phi^{(u)}(\omega)\right|^n d\omega \\ &= \left(\frac{2}{nu}\right)^{\frac{nu}{2}} \frac{u\omega_0^2 exp\left(\frac{nu}{2}\right)}{4} \Gamma\left(\frac{nu}{2}\right), \end{aligned} \tag{17}$$

$$\begin{aligned} D_{III} &= \int_0^\infty (\omega - \omega_m)^2 \left|\Phi^{(u)}(\omega)\right|^n d\omega \\ &= \left(\frac{2}{nu}\right)^{\frac{nu}{2}} \frac{\omega_0^3 exp\left(\frac{nu}{2}\right)}{4} \cdot \\ &\quad \left[\frac{nu+1}{n\sqrt{n}}\Gamma\left(\frac{nu}{2} + \frac{1}{2}\right) - \frac{u^2\sqrt{n}\Gamma^2\left(\frac{nu}{2}\right)}{2\Gamma\left(\frac{nu}{2} + \frac{1}{2}\right)}\right], \end{aligned} \tag{18}$$

the mean frequency of the $n$-th power spectrum of the GSW can be analytically expressed as follows:

$$\begin{aligned} \omega_{n,m} &= \frac{\int_0^\infty \omega \left|\Phi^{(u)}(\omega)\right|^n d\omega}{\int_0^\infty \left|\Phi^{(u)}(\omega)\right|^n d\omega} = \frac{D_{II}}{D_I} \\ &= \frac{u\sqrt{n}\omega_0}{2} \frac{\Gamma\left(\frac{nu}{2}\right)}{\Gamma\left(\frac{nu}{2} + \frac{1}{2}\right)}, \end{aligned} \tag{19}$$

and the standard deviation is:

$$\begin{aligned} \omega_{n,\sigma} &= \left[\frac{\int_0^\infty (\omega - \omega_m)^2 \left|\Phi^{(u)}(\omega)\right|^n d\omega}{\int_0^\infty \left|\Phi^{(u)}(\omega)\right|^n d\omega}\right]^{\frac{1}{2}} \\ &= \sqrt{\frac{D_{III}}{D_I}} \\ &= \frac{\omega_0}{\sqrt{2}} \sqrt{u + \frac{1}{n} - \frac{n}{2}\left[\frac{n\Gamma\left(\frac{nu}{2}\right)}{\Gamma\left(\frac{nu}{2} + \frac{1}{2}\right)}\right]^2}. \end{aligned} \tag{20}$$

It is worth noting here when $n$=2, $\omega_{n,m}$ should be expressed as follows:

$$\omega_{2,m} = \frac{u\Gamma(u)}{\sqrt{2}\Gamma\left(u + \frac{1}{2}\right)}\omega_0, \tag{21}$$

and the standard deviation is:

$$\omega_{2,\sigma} = \frac{\omega_0}{\sqrt{2}} \sqrt{u + \frac{1}{2} - \left[\frac{n\Gamma(u)}{\Gamma\left(u + \frac{1}{2}\right)}\right]^2}, \tag{22}$$

which are the statistical property expressions derived based on the power spectrum of the GSW and the same as the equations (27) and (28) in Wang's literature [26].

With equations (5), (13), (14), (19) and (20), we could set up the frequency coefficients $[\beta_p(u), \beta_c(u), \beta_b(u), \beta_m(u,n), \beta_\sigma(u,n)]^{\mathrm{T}}$, of which the presentation is:

$$\begin{aligned} \begin{bmatrix} \omega_p \\ \omega_c \\ \omega_b \\ \omega_{n,m} \\ \omega_{n,\sigma} \end{bmatrix} &= \omega_0 \begin{bmatrix} \beta_p(u) \\ \beta_c(u) \\ \beta_b(u) \\ \beta_m(u,n) \\ \beta_\sigma(u,n) \end{bmatrix} \\ &= \omega_0 \begin{bmatrix} \sqrt{\frac{u}{2}} \\ \frac{1}{2}\left[\sqrt{-\frac{u}{2}W_{-1}\left(-\frac{1}{2^{2/u}e}\right)} + \sqrt{-\frac{u}{2}W_0\left(-\frac{1}{2^{2/u}e}\right)}\right] \\ \frac{1}{2}\left[\sqrt{-\frac{u}{2}W_{-1}\left(-\frac{1}{2^{2/u}e}\right)} - \sqrt{-\frac{u}{2}W_0\left(-\frac{1}{2^{2/u}e}\right)}\right] \\ \frac{\sqrt{n}u\Gamma\left(\frac{nu}{2}\right)}{2\Gamma\left(\frac{nu}{2} + \frac{1}{2}\right)} \\ \frac{1}{\sqrt{2}}\sqrt{\frac{1}{n} + u - \frac{n}{2}\left[\frac{u\Gamma\left(\frac{nu}{2}\right)}{\Gamma\left(\frac{nu}{2} + \frac{1}{2}\right)}\right]^2} \end{bmatrix}. \end{aligned} \tag{23}$$

Equation (23) establishes the explicit mathematical relationship between the analytic frequency characteristics ($\omega_p$, $\omega_c$ and $\omega_b$) and the statistical properties ($\omega_{n,m}$ and $\omega_{n,\sigma}$) based on the $n$-th power Fourier spectrum of the GSW. It is important to note that the analytic frequency characteristics are not the functions of $n$ and they are not first proposed in this article. They can be found in Wang's literature [26]. The statistical frequency coefficients $\beta_m(u,n)$ and $\beta_\sigma(u,n)$ are the functions of $u$ and $n$. This means that our proposed approach allows the use of any power Fourier spectrum, such as but not limited to the amplitude spectrum ($n$=1) or power spectrum ($n$=2), to estimate the analytic frequency characteristics of the GSW.

As expected, the introduction of parameter $n$ allows us to observe rich variations in the frequency coefficient trends, as shown in Fig.1. The frequency characteristic coefficients ($\beta_p(u)$, $\beta_c(u)$ and $\beta_b(u)$) are depicted by solid curves in different colors, while the statistical frequency coefficients ($\beta_m(u,n)$ and $\beta_\sigma(u,n)$) are depicted by dotted curves.

To demonstrate the influence of different values of $n$ on the statistical frequency coefficient, we plotted the frequency coefficient curves for $n$ = 1.0, 1.5, 2.0, 2.5, and 3.0 as dotted curves with varying intervals in Fig.1. From these curves, we can draw the following conclusions:

(1) All the frequency coefficients are positively correlated with $u$. The statistical frequency coefficients are negatively correlated with $n$. As the value of $n$ increases, the distance between the dotted curves decreases gradually, indicating that the negative correlation decreases with increasing $n$.

(2) The curve of the central frequency coefficient $\beta_c(u)$ falls within the region of the curves of the mean frequency coefficient $\beta_m(u,n)$. This indicates that the mean frequency $\omega_{n,m}$ obtained from the $n$-th power spectrum is approximately equal to the central frequency $\omega_c$. From Fig.1, we can see that the central frequency coefficient is closer to the mean frequency coefficient when $n$=2.0 (power spectrum) than when $n$=1.5. Similarly, the mean frequency estimated from the power spectrum is closer to the central frequency than the one obtained from the amplitude spectrum ($n$=1.0) [26], [35]. Our proposed approach allows us to determine the exact value of $n$ at which the mean frequency is equal to the central frequency, but we do not include this here.

(3) All the frequency coefficient curves calculated from the $n$-th power spectrum have the same trends and relative relationship to each other, including those obtained from the power spectrum [26]. This means that the different power degrees of the spectrum do not alter the variation trend of different frequency parameters, but the weight relationship among them is different. As a result, our proposed method can comprehensively analyze the input signal by analyzing the Fourier spectrum of the signal with different powers and using frequency parameters with varying relationships of weight, making the frequency analysis method more robust.

## IV. Weighting Algorithm of $n$-th Power Fourier Spectrum

To analyze the seismic data, we need to determine the range of values for the variable $n$ to obtain the $n$-th spectrum of the seismic signals. Then, we can use equations (18) and (19) to calculate the mean frequency and its deviation for the spectrum. Finally, using equation (23), we can calculate the ratio of the standard deviation to the mean frequency with respect to $nu$. The resulting ratio can be expressed as follows:

$$\frac{\omega_{n,\sigma}^2}{\omega_{n,m}^2} = \frac{(1+nu)}{nu}\left[\frac{\Gamma\left(\frac{nu}{2}+\frac{1}{2}\right)}{\sqrt{\frac{nu}{2}}\Gamma\left(\frac{nu}{2}\right)}\right]^2 - 1, \tag{24}$$

from which, the fractional value $u$ of Gaussian function could be solved using either a simple iterative method or an asymptotic series method [26]. After obtaining the value of $u$, the next step is to determine the reference frequency $\omega_0$ in order to construct the desired GSW. However, it is essential to consider multiple frequency parameters in order to avoid errors caused by using a single frequency parameter. Therefore, the reference frequency $\omega_0$ can be estimated using the following approach:

$$\omega_0 = \sqrt{\frac{2n}{1+nu}\left(\omega_{n,m}^2 + \omega_{n,\sigma}^2\right)}, \tag{25}$$

in which, the mean frequency $\omega_{n,m}$ and the deviation $\omega_{n,\sigma}$ are both used to help minimize the potential deviation when calculating the reference frequency $\omega_0$.

In field seismic exploration, it is common for the seismic record to contain noise, affecting the accuracy of frequency characteristics in the signal spectrum. The frequency estimation results based on the amplitude spectrum or power spectrum, which is a single power of the Fourier spectrum, are often one-sided and may not be reliable.

Therefore, it is necessary to weight the calculated fractional value $u_{cal}$ by different $n$-th Fourier spectra to obtain a weighted fractional value $u_{ave}$. Using this weighted value $u_{ave}$ can often provide better robustness and noise immunity when calculating the reference frequency $\omega_0$ and predicting the GSW.

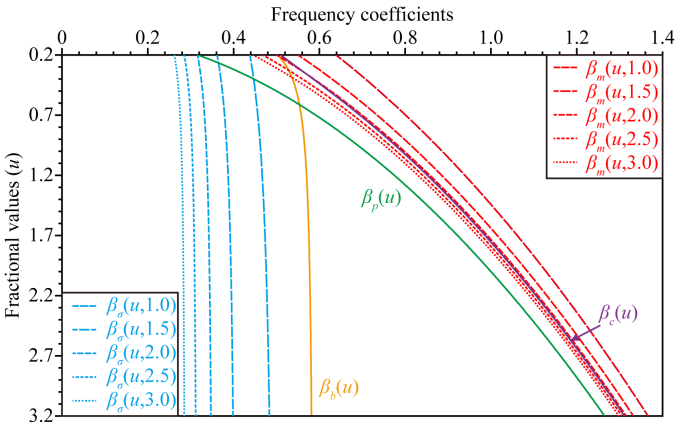


Fig. 1. Frequency coefficients $\beta_p(u)$, $\beta_c(u)$, $\beta_b(u)$, $\beta_m(u,n)$ and $\beta_\sigma(u,n)$ versus the power value of $n$ and the fractional value of $u$.

## V. Numerical Experiments

### A. Frequency Analysis of Ideal GSW

To demonstrate the effectiveness of the proposed method, we first utilize different fractional derivatives of a Gaussian

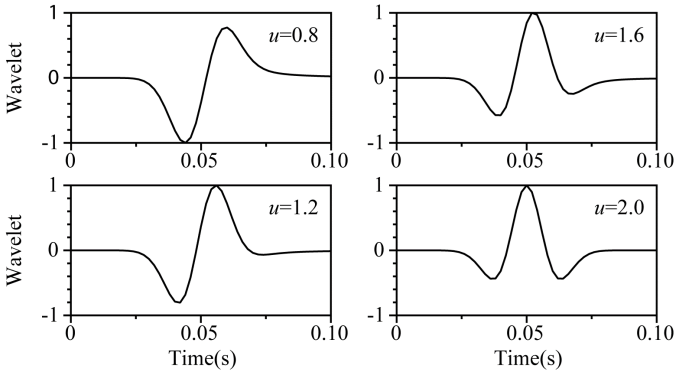


Fig. 2. The GSW defined by different fractional derivatives of a Gaussian function.

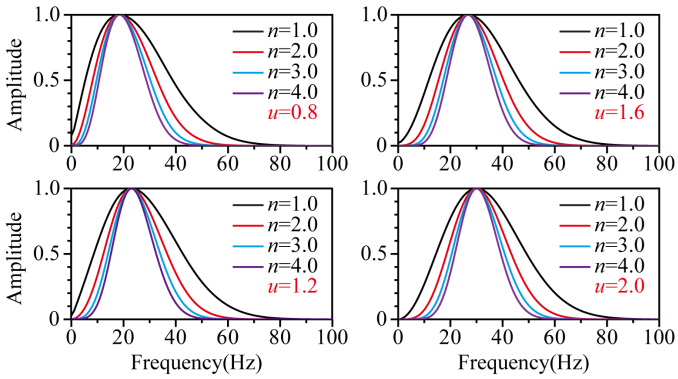


Fig. 3. The comparison of the $n$-th power spectra of GSW.

function to construct the GSW, as shown in Fig.2. In this figure, the fraction $u$ ranges from 0.6 to 2.0. By changing the value of the fractional derivative of the Gaussian function, we can obtain wavelets with different phases. We then perform the the GSW's Fourier transform and calculate the complex data's modulus to the $n$-th power to bring the $n$-th Fourier spectrum of the GSW. It's easy to infer that as $n$ increases, the shape of the Fourier spectrum will be progressively narrower and more focused around the peak frequency. In Fig.3, we show the $n$-th power of the Fourier spectra of the GSW with a reference frequency of $\omega_0 = 60\pi$, which illustrates this phenomenon more clearly.

Using the $n$-th Fourier spectra data, we can calculate the mean frequency $\omega_{n,m}$ and standard deviation $\omega_{n,\sigma}$ using equations (18) and (19), and then utilize equation (24) to calculate the fractional derivative $u$, as shown in Fig.4. For GSW of different phases, the calculated value of $u_{cal}$ remains fairly constant as $n$ changes, indicating that the correct fractional derivative $u$ of the Gaussian function can be accurately calculated under ideal conditions, without noise in the seismic data.

### B. Noise Immunity Test

To further examine the noise immunity of the proposed approach, we start with a synthesized first arrival record

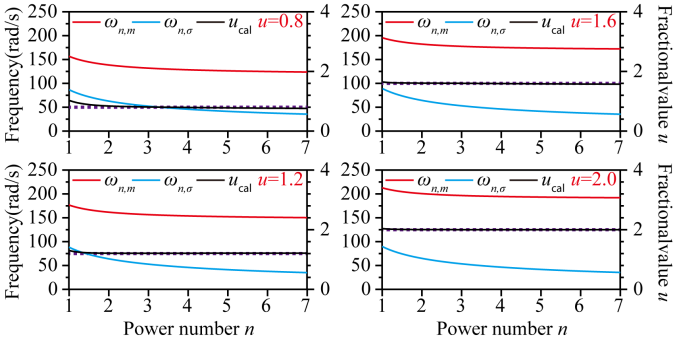


Fig. 4. The statistical properties($\omega_{n,m}$ and $\omega_{n,\sigma}$) and $u_{cal}$ calculated by the $n$-th Fourier spectra of the ideal GSW.

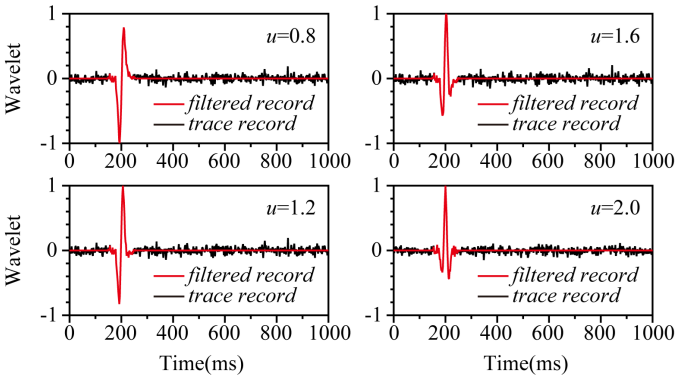


Fig. 5. The trace record synthesized with GSW (including the Gaussian noise with a SNR of 15) and the filtered record by a cosine-square tapering.

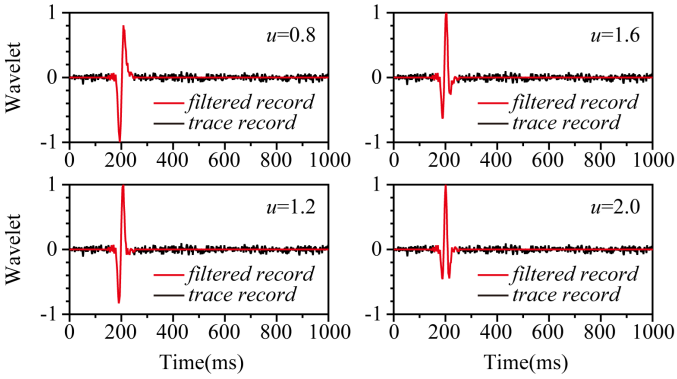


Fig. 6. The trace record synthesized with GSW (including the Gaussian noise with a SNR of 20) and the filtered record by a cosine-square tapering.

using the GSW with a reference frequency of $\omega_0 = 60\pi$, as mentioned in the previous section. We then add Gaussian noise with signal-to-noise ratios (SNR) of 15 and 20. The noise-containing data are shown by the solid black curves in Fig.5 and 6. To simulate the actual workflow, we pick up the first arrival based on the travel time and apply a cosine-square tapering to suppress unwanted seismic signals that are not part of the first arrival. The seismic signals after this processing are shown as solid red curves in Fig.5 and 6.

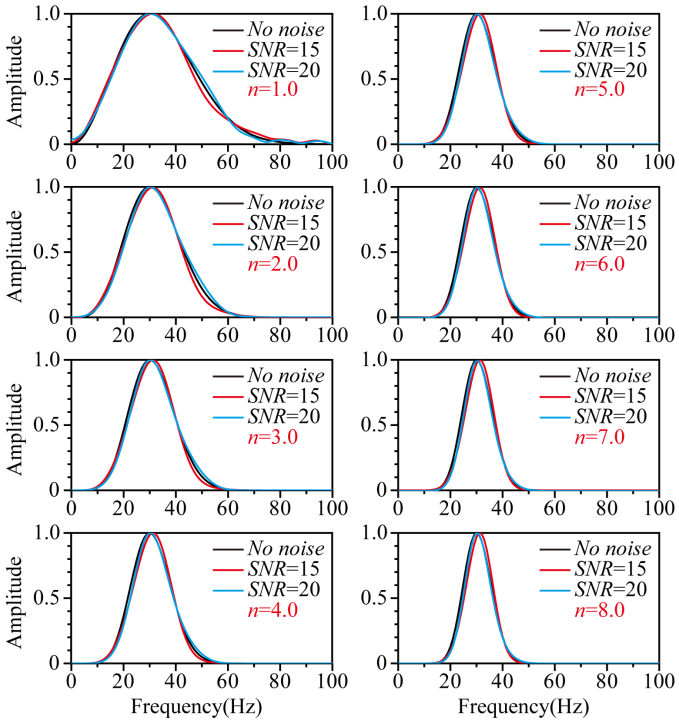


Fig. 7. The $n$-th Fourier spectra of the filtered noise-containing (SNR=15 and 20) and noise-free first-arrival records.

We also perform $n$-th Fourier spectrum calculation on the above noise-containing first-arrival records (synthesized by the GSW with $u$=2.0). The results are shown by the solid red (SNR=15) and blue (SNR=20) curves in Fig.7. For comparison, we also include the $n$-th Fourier spectrum curves of the GSW without noise by the solid black curves in Fig.7.

The Fourier spectra of the picked first arrivals with Gaussian noise are distorted compared to the noise-free synthetic seismic records. When $n$ is relatively small, the energy in the Fourier spectrum exhibits a "defocusing" trend, meaning that the effective frequency band has a very small proportion of energy. The effect of noise on each Fourier spectrum is more pronounced, making it difficult to obtain accurate frequency information and predict the GSW using the Fourier spectra of smaller power number. However, when $n$ is relatively large, the corresponding $n$-th Fourier spectra exhibit a "focusing" phenomenon. As a result, there is no significant difference in shape between the $n$-th Fourier spectra of noise-containing and noise-free first-arrival records. However, as $n$ increases, the contribution of low-frequency and high-frequency components in the signals is significantly reduced, and the frequency information of the "focus region" near the peak frequency does not fully represent all the frequency characteristics of the first-arrival recordings. Therefore, relying solely on a specific $n$ to obtain the $n$-th Fourier spectrum and the calculated frequency parameter is not as reliable as one might think. To verify this point, we plot the $\omega_\sigma$, $\omega_m$ and $u_{cal}$ calculated from the $n$-th Fourier spectra for different $n$ values, as shown in Fig.8 (SNR=15) and Fig.9 (SNR=20). In these figures, we can see that the calculated $\omega_m$, $\omega_d$ and $u$ tend to change with the change of $n$. When $n$ is small, the "defocusing" mentioned above leads to larger values of $\omega_\sigma$ and $\omega_m$, which in turn leads to a calculated $u_{cal}$ value (shown as the solid black curves in Figs.8 and 9) that is less than the correct $u$ value (shown as the dotted red curves in Figs.8 and 9). As the value of $n$ increases, the calculated $u_{cal}$ value gradually becomes stable. However, there is still a discrepancy with the correct $u$, and we cannot arbitrarily assume that the higher value of $n$, the more accurate the calculation is. Therefore, using an average of $u_{cal}$ values calculated from different $n$-th Fourier spectra, known as $u_{ave}$, can improve the robustness and noise immunity of the GSW estimation method.

In this test, we use the range of $n$ from 3.0 to 7.0 to calculate the average weighting $u_{ave}$. It is worth noting that the selection of the range of $n$ is an empirical parameter, and the same range is used in the subsequent experiments in this paper. The $u_{ave}$ is shown by the solid green curves in Figs.8 and 9. It can be seen that the weighting $u_{ave}$ value is very close to the correct value of $u$, even when the data includes noise. The calculation accuracy is significantly higher than when conventionally used the amplitude spectrum ($n$=1.0) or power spectrum ($n$=2.0) . While it may be possible to find a specific value of $n$ that results in a calculated $u_{cal}$ value closest to the correct value of $u$ for each trace record data, it is not possible to predict this specific value of $n$ in the actual workflow. Therefore, the weighting $u_{ave}$ method proposed in this paper often achieves higher precision and robustness. Next, we substitute the $u_{ave}$ into equation (25) and continue to calculate $\omega_0$ from the $n$-th Fourier spectrum. The results are shown by the solid yellow curves in Fig.8 and 9. Similarly, it is challenging to obtain relatively accurate $\omega_0$ by relying on the Fourier spectrum of a single power degree. Therefore, it is also necessary to perform the weighting calculation on $\omega_0$. In this experiment, we again use the $n$-th Fourier spectrum in the range of 3.0 to 7.0. The computed $\omega_{0-cal}$ is weighted proportionally to obtain $\omega_{0-ave}$, as shown by the solid brown curves in Fig.8 and 9. The experimental results show that the $\omega_{0-ave}$ obtained through weighting calculations is close to the theoretically correct value of $\omega_0$.

By using the weighting $u_{ave}$ and $\omega_{0-ave}$, along with the picked first arrival time $\tau_0$, we construct the Fourier spectrum data according to equation (3) and perform the inverse Fourier transform to obtain the predicted time-domain seismic signals, as shown in Fig.(10). From this, we can see that the seismic record constructed using the GSW synthesized by the proposed method has a high correlation coefficient with the test data (parameter '$c$' in Fig.(10)), demonstrating the effectiveness and strong noise resistance of the proposed method.

### C. Field Signal Experiment

In this section, we test our approach using field VSP records. We select 10 traces of pressure data from a VSP common shot gather, with 10 receivers between depths of 750 m and 840 m. Fig.11 displays the 10 trace records and the frequency analysis results using the proposed method. From this, we can observe

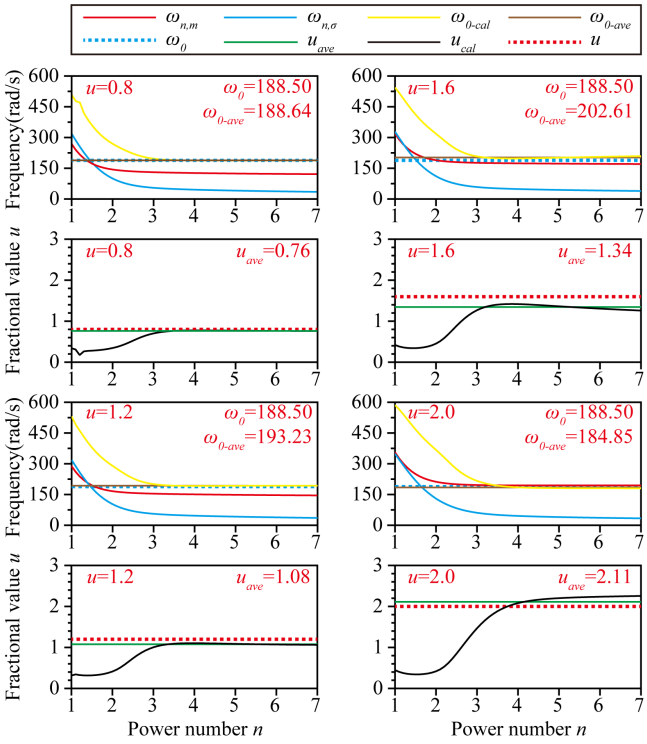


Fig. 8. The frequency parameters calculated by the $n$-th Fourier spectra of the filtered noise-containing (SNR=15) first-arrival records.

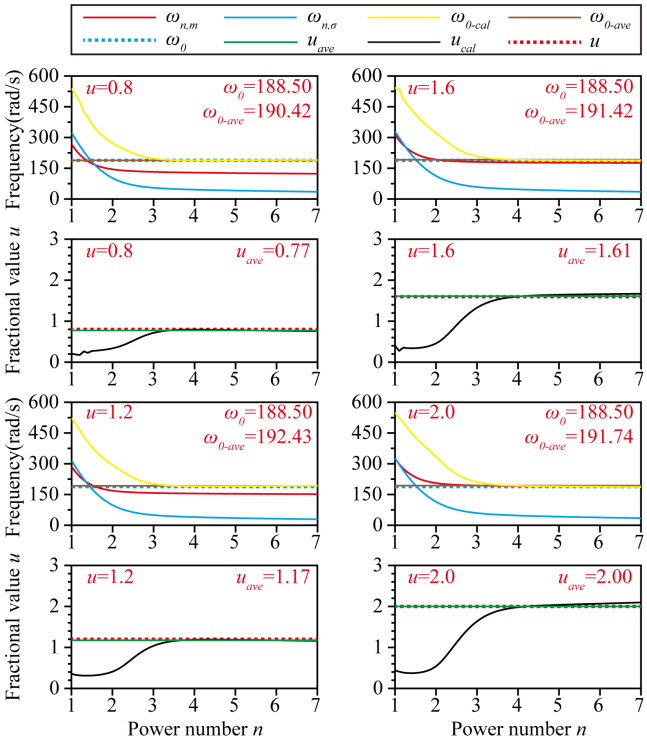


Fig. 9. The frequency parameters calculated by the $n$-th Fourier spectra of the filtered noise-containing (SNR=20) first-arrival records.

the following:

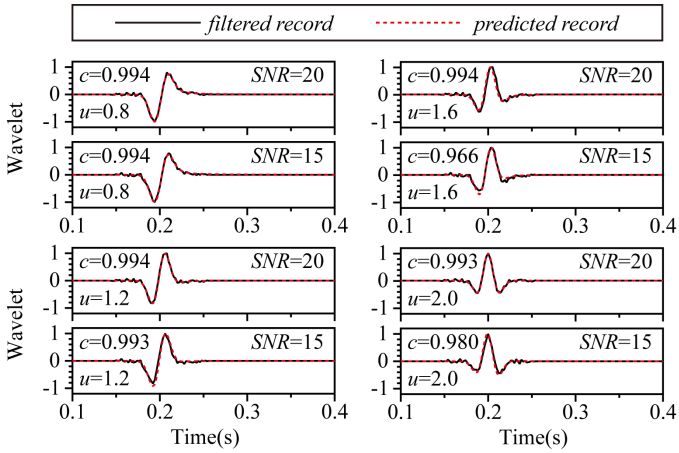


Fig. 10. Comparison between the synthetic noise-containing records and the predicted records with weighting $u_{ave}$ and $\omega_{0-ave}$.

(1) The waveforms between 250-400 ms including the first arrivals are shown in the "Wavelets" column. The solid gray curves represent the initial field trace records, while the solid black curves show the filtered trace records using a cosine-square tapering, suppressesing unwanted seismic signals such as multiples and reflections. We compared the matching of the field signals and GSW predicted using the amplitude spectrum, power spectrum and proposed method, shown as solid red, blue and green curves, respectively. In this experiment, we still use the range of $n$ from 3.0 to 7.0 for the weighting calculation of the Fourier spectra. Although the GSW calculated using the amplitude or power spectrum can match well with the field signals. The method proposed in this paper avoids the contingency of frequency estimation by using the above two Fourier spectra in the weighting calculation of different power Fourier spectra, which theoretically performs better than the first two.

(2) In the "Correlation" column, we also plotted the correlation curves between the filtered trace record and the GSW calculated using the amplitude, power spectrum and the proposed method. These correlation coefficients further verify the points made above.

(3) From the "$\omega_0$ and $\omega_m$" and "$u$" columns, we can see a high correlation between $\omega_m$ and $u$ regardless of which Fourier spectrum is used, which is similar to the conclusion reached in Wang's article [26]. Additionally, the values of $u$ calculated using the amplitude and power spectra are smaller than the proposed method, which is more accurate based on the matching between the GSW and the field signals. Lastly, the differences between $\omega_0$ calculated using the amplitude, power, and $n$-th spectrum are not as significant as in the previous test. The author believes that this is because the noise type in the field trace record is different from the previous test.

### D. Necessary Preprocessing

In order to clearly express the proposed method, we have avoided some preprocessing steps by selecting a safe window in the above experiments. However, it's important to note that

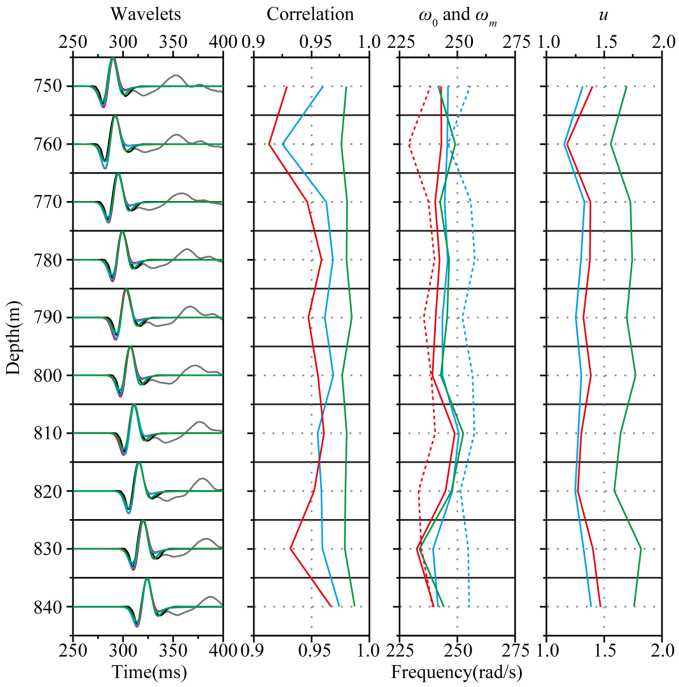


Fig. 11. GSW and frequency analysis comparisons from amplitude, power and $n$-th Fourier spectra of the field VSP records.

the proposed method is a type of spectral fitting method that is sensitive to the shape of the Fourier spectrum [25]. This means that some of the earth's response may be unavoidable and could potentially influence the statistical properties inferred from field data. Therefore, in actual application scenarios, it is necessary to apply some preprocessing to the input signal to make it suitable for use with the proposed method.

For example, when using the proposed method for stable Q analysis on VSP data (a typical application scenario [6]), effective first arrival extraction processing is essential for wavelet estimation. To obtain the downgoing wavetrains, we should first apply median filtering, and then use a cosine-square taper according to the first arrival travel time to suppress late arrivals, which are mostly made up of waveforms of multiples generated from the free surface [6], [26]. Only then can we use the effective first arrival signal with the proposed method. In other seismic data application scenarios, there are also unique preprocessing steps, which will not be described in this paper.

## VI. Conclusions and Discussion

The frequency analysis method based on the amplitude or power spectrum can be used to construct the GSW matching well with seismic recording signals. The proposed approach builds upon this by using $n$-th power Fourier spectra to compute the frequency properties of the GSW, which is a theoretical extension of the power number of the Fourier spectrum from 1 or 2 to an arbitrary value. This method provides analytical expressions for the frequency properties of the GSW, such as the central frequency, the bandwidth, the mean frequency, and the deviation, creating a more holistic and straightforward relation between frequency characteristics and statistical properties. Based on this, the frequency properties of the GSW can be seen as a function of both the fractional value of $u$ and the power value of $n$, rather than just being related to the value of $u$. The proposed frequency analysis technique based on the $n$-th power Fourier spectra is not contradictory to the method based on the power spectrum that has been published on some literatures [26], [35], [38]. In fact, it provides a more comprehensive frequency analysis strategy. The proposed method can achieve higher robustness and noise resistance by weighting the fractional derivatives $u_{ave}$ of the Gaussian function, as both theoretical and field trace data have shown.

Generalized seismic wavelet is a flexible method for defining wavelets. It can be used not only to extract seismic wavelets from first arrival data, but also to play a crucial role in the seismic wavelet extraction method based on reflected data. However, current methods for estimating frequency parameters still rely on the amplitude spectrum or power spectrum [24], [25], [39]. The proposed plan has the potential to be extended to these methods and provide more stable and accurate algorithm support. This is also the future direction of this paper.

## Acknowledgments

This work was supported in part by the Project of the National Natural Science Foundation of China (Grant No. 41930431, 41974116, 42274171 and 41904121), Outstanding Youth Project of Natural Science Foundation of Heilongjiang Province (YQ2021D008), CNPC Innovation Found (2021DQ02-0302), China Postdoctoral Science Foundation (Grant No. 2019M651253), Heilongjiang Provincial Postdoctoral Science Foundation (Grant No. LBH-Z18040), "Key Laboratory of Formation Mechanism and Resource Evaluation of Oil and Gas Reservoirs in Heilongjiang Province" Open fund project (Grant No. KL20190105), Pilot Innovation Fund of Northeastern Petroleum University (2021YDL-04), and Universities Reformation and Development Personnel Training Supporting Project from Central Authorities (140119001).

## Appendix
## Derivation of the Definite Integrals $D_I$, $D_{II}$ and $D_{III}$

Firstly, we need to define $x = \frac{\sqrt{n}\omega}{\omega_0}$, $y = x^2 = \frac{n\omega^2}{\omega_0^2}$. According to the concept and property of the Gamma function, we can obtain:

$$\int_0^\infty x^{nu} exp\left(-x^2\right) dx = \frac{1}{2}\Gamma\left(\frac{nu}{2}+\frac{1}{2}\right), \tag{A.1}$$

$$\begin{aligned}\int_0^\infty y^{\frac{nu+1}{2}} exp\left(-y\right) dy &= \Gamma\left(\frac{nu+1}{2}+1\right) \\ &= \frac{nu+1}{2}\Gamma\left(\frac{nu+1}{2}\right).\end{aligned} \tag{A.2}$$

The derivation process of equation (16) is as follows:

$$\begin{aligned} D_I &= \int_0^\infty |\Phi^{(u)}(\omega)|^n d\omega \\ &= \int_0^\infty \left(\frac{2}{u}\right)^{\frac{nu}{2}} \frac{\omega^{nu}}{\omega_0^{nu}} exp\left(-\frac{n\omega^2}{\omega_0^2} + \frac{nu}{2}\right) d\omega \\ &= \left(\frac{2}{nu}\right)^{\frac{nu}{2}} \frac{exp\left(\frac{nu}{2}\right)\omega_0}{\sqrt{n}} \int_0^\infty \left(\frac{\sqrt{n}\omega}{\omega_0}\right)^{nu} \cdot \\ &\quad exp\left[-\left(\frac{\sqrt{n}\omega}{\omega_0}\right)^2\right] d\left(\frac{\sqrt{n}\omega}{\omega_0}\right) \\ &= \left(\frac{2}{nu}\right)^{\frac{nu}{2}} \frac{exp\left(\frac{nu}{2}\right)\omega_0}{\sqrt{n}} \int_0^\infty x^{nu} exp\left(-x^2\right) dx \\ &= \left(\frac{2}{nu}\right)^{\frac{nu}{2}} \frac{exp\left(\frac{nu}{2}\right)\omega_0}{2\sqrt{n}} \Gamma\left(\frac{nu}{2} + \frac{1}{2}\right). \end{aligned} \tag{A.3}$$

The derivation process of equation (17) is as follows:

$$\begin{aligned} D_{II} &= \int_0^\infty \omega |\Phi^{(u)}(\omega)|^n d\omega \\ &= \left(\frac{2}{u}\right)^{\frac{nu}{2}} exp\left(\frac{nu}{2}\right) \int_0^\infty \omega \left(\frac{\omega}{\omega_0}\right)^{nu} \cdot \\ &\quad exp\left[-\left(\frac{\sqrt{n}\omega}{\omega_0}\right)^2\right] d\omega \\ &= \left(\frac{2}{nu}\right)^{\frac{nu}{2}} \frac{\omega_0^2 exp\left(\frac{nu}{2}\right)}{2n} \cdot \\ &\quad \int_0^\infty \left(\frac{n\omega^2}{\omega_0^2}\right)^{\frac{nu}{2}} exp\left(-\frac{n\omega^2}{\omega_0^2}\right) d\left(\frac{n\omega^2}{\omega_0^2}\right) \\ &= \left(\frac{2}{nu}\right)^{\frac{nu}{2}} \frac{\omega_0^2 exp\left(\frac{nu}{2}\right)}{2n} \int_0^\infty y^{\frac{nu}{2}} exp(-y)\, dy \\ &= \left(\frac{2}{nu}\right)^{\frac{nu}{2}} \frac{\omega_0^2 exp\left(\frac{nu}{2}\right)}{2n} \Gamma\left(\frac{nu}{2} + 1\right) \\ &= \left(\frac{2}{nu}\right)^{\frac{nu}{2}} \frac{u\omega_0^2 exp\left(\frac{nu}{2}\right)}{4} \Gamma\left(\frac{nu}{2}\right). \end{aligned} \tag{A.4}$$

The derivation process of equation (18) is as follows:

$$\begin{aligned} D_{III} &= \int_0^\infty (\omega - \omega_m)^2 |\Phi^{(u)}(\omega)|^n d\omega \\ &= \int_0^\infty \omega^2 |\Phi^{(u)}(\omega)|^n d\omega \\ &\quad - \int_0^\infty 2\omega\omega_m |\Phi^{(u)}(\omega)|^n d\omega \\ &\quad + \int_0^\infty {\omega_m}^2 |\Phi^{(u)}(\omega)|^n d\omega \\ &= \int_0^\infty \omega^2 |\Phi^{(u)}(\omega)|^n d\omega - 2\omega_m D_{II} + {\omega_m}^2 D_I. \end{aligned} \tag{A.5}$$

To further deduce equation (A.5), we need to solve the following definite integral:

$$\begin{aligned} &\int_0^\infty \omega^2 |\Phi^{(u)}(\omega)|^n d\omega \\ &= \int_0^\infty \omega^2 \left(\frac{2}{u}\right)^{\frac{nu}{2}} \frac{\omega^{nu}}{\omega_0^{nu}} exp\left(-\frac{n\omega^2}{\omega_0^2} + \frac{nu}{2}\right) d\omega \\ &= \left(\frac{2}{nu}\right)^{\frac{nu}{2}} \frac{\omega_0^3 exp\left(\frac{nu}{2}\right)}{2n\sqrt{n}} \cdot \\ &\quad \int_0^\infty \left(\frac{n\omega^2}{\omega_0^2}\right)^{\frac{nu+1}{2}} exp\left(-\frac{n\omega^2}{\omega_0^2}\right) d\left(\frac{n\omega^2}{\omega_0^2}\right) \\ &= \left(\frac{2}{nu}\right)^{\frac{nu}{2}} \frac{\omega_0^3 exp\left(\frac{nu}{2}\right)}{2n\sqrt{n}} \int_0^\infty y^{\frac{nu+1}{2}} exp(-y) dy \\ &= \left(\frac{2}{nu}\right)^{\frac{nu}{2}} \frac{\omega_0^3 exp\left(\frac{nu}{2}\right)}{2n\sqrt{n}} \Gamma\left(\frac{nu+1}{2} + 1\right) \\ &= \left(\frac{2}{nu}\right)^{\frac{nu}{2}} \frac{(nu+1)\omega_0^3 exp\left(\frac{nu}{2}\right)}{4n\sqrt{n}} \Gamma\left(\frac{nu+1}{2}\right). \end{aligned} \tag{A.6}$$

Take equations (A.3), (A.4), and (A.6) into equation (A.5), $D_{III}$ could be expressed as follows:

$$\begin{aligned} D_{III} &= \left(\frac{2}{nu}\right)^{\frac{nu}{2}} \frac{\omega_0^3 exp\left(\frac{nu}{2}\right)}{4} \cdot \\ &\quad \left[\frac{nu+1}{n\sqrt{n}} \Gamma\left(\frac{nu}{2} + \frac{1}{2}\right) - \frac{u^2\sqrt{n}\Gamma^2\left(\frac{nu}{2}\right)}{2\Gamma\left(\frac{nu}{2} + \frac{1}{2}\right)}\right] \end{aligned} \tag{A.7}$$

## REFERENCES


[1] N. Ricker, "Further developments in the wavelet theory of seismogram structure," *Bulletin of the Seismological Society of America*, vol. 33, no. 3, pp. 197–228, 1943.

[2] ——, "Wavelet functions and their polynomials," *Geophysics*, vol. 9, no. 3, pp. 314–323, 1944.

[3] ——, "The form and laws of propagation of seismic wavelets." *Geophysics*, vol. 18, no. 1, pp. 10–40, 1953.

[4] J. Hosken, "Ricker wavelets in their various guises," *First Break*, vol. 6, no. 1, 1988.

[5] Y. Wang, "Q analysis on reflection seismic data," *Geophysical Research Letters*, vol. 31, no. 17, 2004.

[6] ——, "Stable q analysis on vertical seismic profiling data," *Geophysics*, vol. 79, no. 4, pp. D217–D225, 2014.

[7] N. Wang, G. Xing, T. Zhu, H. Zhou, and Y. Shi, "Propagating seismic waves in vti attenuating media using fractional viscoelastic wave equation," *Journal of Geophysical Research: Solid Earth*, vol. 127, no. 4, p. e2021JB023280, 2022.

[8] Z. Ren, X. Dai, and Q. Bao, "Source wavefield reconstruction based on an implicit staggered-grid finite-difference operator for seismic imaging," *Petroleum Science*, vol. 19, pp. 2095–2106, 2022.

[9] L. Song, Y. Shi, W. Liu, and Q. Zhao, "Elastic reverse time migration for weakly illuminated structure," *Applied Sciences*, vol. 12, no. 10, p. 5264, 2022.

[10] X. Guo, H. Liu, and Y. Shi, "Modified interferometric imaging condition for reverse-time migration," *Exploration Geophysics*, vol. 49, no. 2, pp. 202–212, 2018.

[11] W. Zhang and Y. Shi, "Imaging conditions for elastic reverse time migration," *Geophysics*, vol. 84, no. 2, pp. S95–S111, 2019.

[12] W. Zhang, J. Gao, Z. Gao, and Y. Shi, "2d and 3d amplitude-preserving elastic reverse time migration based on the vector-decomposed p-and s-wave records," *Geophysical Prospecting*, vol. 68, no. 9, pp. 2712–2737, 2020.

[13] Z. Ren, Q. Bao, and S. Xu, "Memory-efficient source wavefield reconstruction and its application to 3d reverse time migration," *Geophysics*, vol. 87, no. 1, pp. S21–S34, 2022.

[14] W. Zhang, J. Gao, Y. Cheng, C. Su, H. Liang, and J. Zhu, "3-d image-domain least-squares reverse time migration with l1 norm constraint and total variation regularization," *IEEE Transactions on Geoscience and Remote Sensing*, vol. 60, pp. 1–14, 2022.

[15] X. Guo, H. Liu, Y. Shi, W. Wang, and Z. Zhang, "Improving waveform inversion using modified interferometric imaging condition," *Acta Geophysica*, vol. 66, no. 1, pp. 71–80, 2018.
[16] W. Zhang and J. Gao, "Deep-learning full-waveform inversion using seismic migration images," *IEEE Transactions on Geoscience and Remote Sensing*, vol. 60, pp. 1–18, 2021.
[17] Z. Ren, Q. Bao, and B. Gu, "Time-dispersion correction for arbitrary even-order lax-wendroff methods and the application on full-waveform inversion," *Geophysics*, vol. 86, no. 5, pp. T361–T375, 2021.
[18] E. Bianco, "Tutorial: Wavelet estimation for well ties," *The Leading Edge*, vol. 35, no. 6, pp. 541–543, 2016.
[19] L. R. Lines and S. Treitel, "Wavelets, well logs and wiener filters," *First Break*, vol. 3, pp. 9–14, 1985.
[20] I. A. de Macedo and J. J. S. de Figueiredo, "On the seismic wavelet estimative and reflectivity recovering based on linear inversion: Well-to-seismic tie on a real data set from viking graben, north sea," *Geophysics*, vol. 85, no. 5, pp. D157–D165, 2020.
[21] M. D. Sacchi and T. J. Ulrych, "Nonminimum-phase wavelet estimation using higher order statistics," *The Leading Edge*, vol. 19, no. 1, pp. 80–83, 2000.
[22] A. T. Walden and R. E. White, "Seismic wavelet estimation: A frequency domain solution to a geophysical noisy input-output problem," *IEEE transactions on Geoscience and Remote Sensing*, vol. 36, no. 1, pp. 287–297, 1998.
[23] R. Zhang and Z. Deng, "A depth variant seismic wavelet extraction method for inversion of poststack depth-domain seismic data," *Geophysics*, vol. 83, no. 6, pp. R569–R579, 2018.
[24] S. Ker and Y. Le Gonidec, "Filtering of a ricker wavelet induced by anelastic seismic wave propagation and reflection," *Journal of Geophysics and Engineering*, vol. 17, no. 5, pp. 838–851, 2020.
[25] J. Zhang, X. Chen, W. Jiang, Y. Liu, and H. Xu, "Estimation of the depth-domain seismic wavelet based on velocity substitution and a generalized seismic wavelet model," *Geophysics*, vol. 87, no. 2, pp. R213–R222, 2022.
[26] Y. Wang, "Generalized seismic wavelets," *Geophysical Journal International*, vol. 203, no. 2, pp. 1172–1178, 2015.
[27] Y. Rao, Y. Guo, and D. Xu, "Detecting karst voids based on dominant frequencies of seismic profiles," *Pure and Applied Geophysics*, vol. 178, no. 8, pp. 3057–3067, 2021.
[28] D. Yang, J. Liu, J. Li, and D. Liu, "Q-factor estimation using bisection algorithm with power spectrumq estimation by bisection algorithm," *Geophysics*, vol. 85, no. 3, pp. V233–V248, 2020.
[29] H. Hardy, R. A. Beier, and J. D. Gaston, "Frequency estimates of seismic traces," *Geophysics*, vol. 68, no. 1, pp. 370–380, 2003.
[30] S. Huo, "Frequency estimates of seismic traces," *Geophysics*, vol. 80, no. 5, pp. V115–V118, 2015.
[31] S. S. Ahmad, R. J. Brown, A. Escalona, and B. O. Rosland, "Frequency-dependent velocity analysis and offset-dependent low-frequency amplitude anomalies from hydrocarbon-bearing reservoirs in the southern north sea, norwegian sectorlow-frequency analysis," *Geophysics*, vol. 82, no. 6, pp. N51–N60, 2017.
[32] A. J. Carter and J.-M. Kendall, "Attenuation anisotropy and the relative frequency content of split shear waves," *Geophysical Journal International*, vol. 165, no. 3, pp. 865–874, 2006.
[33] J. H. Lambert, "Observationes variae in mathesin puram," *Acta Helvetica*, vol. 3, no. 1, pp. 128–168, 1758.
[34] R. M. Corless, G. H. Gonnet, D. E. Hare, D. J. Jeffrey, and D. E. Knuth, "On the lambertw function," *Advances in Computational mathematics*, vol. 5, no. 1, pp. 329–359, 1996.
[35] Y. Wang, "Frequencies of the ricker wavelet," *Geophysics*, vol. 80, no. 2, pp. A31–A37, 2015.
[36] A. E. Barnes, "Instantaneous spectral bandwidth and dominant frequency with applications to seismic reflection data," *Geophysics*, vol. 58, no. 3, pp. 419–428, 1993.
[37] M. Caputo, "Linear models of dissipation whose q is almost frequency independent—ii," *Geophysical Journal International*, vol. 13, no. 5, pp. 529–539, 1967.
[38] Y. Wang, "The ricker wavelet and the lambert w function," *Geophysical Journal International*, vol. 200, no. 1, pp. 111–115, 2015.
[39] Y. Jiang, S. Cao, S. Chen, and D. Zheng, "A blind nonstationary deconvolution method for multichannel seismic data," *Exploration Geophysics*, vol. 52, no. 3, pp. 245–257, 2021.